

# Microscopic resolution of the interplay of Kondo screening and superconducting pairing

J. Bauer<sup>1,2</sup>, J. I. Pascual<sup>3</sup>, and K. J. Franke<sup>3,4</sup>

<sup>1</sup>Max-Planck Institute for Solid State Research, Heisenbergstr.1, 70569 Stuttgart, Germany

<sup>2</sup>Department of Physics, Harvard University, Cambridge, Massachusetts 02138, USA

<sup>3</sup>Freie Universität Berlin, Institut für Experimentalphysik, Arnimallee 14, 14195 Berlin, Germany and

<sup>4</sup>Technische Universität Berlin, Institut für Festkörperphysik, Hardenbergstraße 36, 10623 Berlin, Germany

(Dated: August 17, 2012)

Magnetic molecules adsorbed on a superconductor give rise to a local competition of Cooper pair and Kondo singlet formation inducing subgap bound states. For manganese-phthalocyanine molecules on a Pb(111) substrate, featuring numerous different Kondo scales, such states are resolved by scanning tunneling spectroscopy. We show that numerical renormalization group calculations for an effective one channel Anderson impurity model explain the energy and weight of the bound states very well. The application of the model and its parameters are justified by scaling arguments.

PACS numbers: 72.10.Fk, 72.15.Qm, 75.20.Hr, 73.20.-r, 73.20.Hb, 74.81.-g

Magnetic atoms and molecules adsorbed on superconducting surfaces allow for the microscopic observation of the fascinating interplay of Cooper pair and Kondo singlet formation [1–10]. The ground state (GS) of such a combined system has been predicted to be either a Kondo screened singlet state ( $S = 0$ ), if the Kondo scale  $k_B T_K$  is much larger than the superconducting pairing energy  $\Delta_{sc}$ , or an unscreened multiplet state ( $S > 0$ ) for  $k_B T_K \ll \Delta_{sc}$ . Characteristic features include subgap bound states (BS) - often called Shiba states. For the singlet GS with screened impurity spin, the BS are  $S > 0$  excitations, where the Kondo singlet is broken, and for the multiplet GS the BS are singlet excitations including Kondo screening. When the energy scale for Kondo singlet formation becomes smaller and comparable with the Cooper pairing energy,  $k_B T_K \sim \Delta_{sc}$ , the BS energy  $E_b \rightarrow 0$ , and GS and BS cross. At this point a quantum phase transition from  $S = 0$  to  $S > 0$  occurs. The scattering and Cooper pair breaking effect is expected to behave like  $1 - (E_b/\Delta_{sc})^2$  and thus most effective here leading to a strong suppression of the superconducting  $T_c$  for larger impurity concentrations [4, 5, 7].

For a long time the accurate resolution of the subgap BS and their dependence on  $T_K$  and  $\Delta_{sc}$  have remained elusive. Recently, the BS have been analyzed in tunable mesoscopic superconductor-quantum dot-normal lead structures [11]. Scanning tunneling microscopy (STM) has been used to detect the local influence of single magnetic atoms on a superconducting substrate [12]. To study the interplay, an experiment with variable magnetic interaction strengths is desirable. Manganese-phthalocyanine (MnPc) molecules on a Pb(111) substrate forms a Moire-like superstructure. Due to a large number of different adsorption sites, which lead to varying Kondo coupling strengths  $J$ , one can study different values of  $T_K$  and access the regime  $k_B T_K \sim \Delta_{sc}$  [13]. Tunneling spectroscopy on different Mn sites reveals varying  $E_b$  and the occurrence of the predicted GS transition [13].

In spite of the complexity of MnPc the observations could be understood qualitatively by the physics of quantum impurity models [13]. However, the question whether the experimental data agrees quantitatively with predictions from an effective one channel Anderson impurity model (AIM), which has been subject of the theoretical literature for decades, has remained open. To provide an answer is a crucial step to unite theory and experiment, and to validate the microscopic understanding of the physical processes of screening and pair breaking. Relevant quantities to compare include the value  $R_{K,sc} = k_B T_K/\Delta_{sc}$  for the occurrence of the GS transition and the positions  $E_b$  and weights  $w_b$  of the BS. In this work we provide a detailed comparison of the experimental observations with numerical renormalization group (NRG) [14–18] calculations, which are known to capture the Kondo effect accurately. Many other methods have been used to describe theoretically impurities in superconductors on a microscopic scale, however, most of them contain mean field aspects like classical spins, such that the Kondo effect is not treated reliably [2–6, 19–21]. For an appropriate parameter regime, we find good agreement with the experimental data, which supports the description in terms of an effective one channel model. Furthermore, we derive the effective model from the more general situation using scaling arguments.

MnPc molecules (see Fig. 1(a)) have been deposited on an atomically clean Pb(111) substrate at room temperature under ultra-high vacuum conditions. STM at 4.5 K resolves highly ordered islands (Fig. 1(b)). Tunneling spectroscopy has been used to resolve the superconducting gap structure and its subgap states, as well as Kondo resonances on different molecules. The superconducting state of the Pb(111) substrate and Pb tip shows as pronounced differential conductance peaks at  $E = \pm 2\Delta_{sc}$  with  $\Delta_{sc} = 1.1 meV$ .

On the Mn sites, we identify a broad peak around the Fermi energy (see Fig. 3(b)), which can be fitted by two

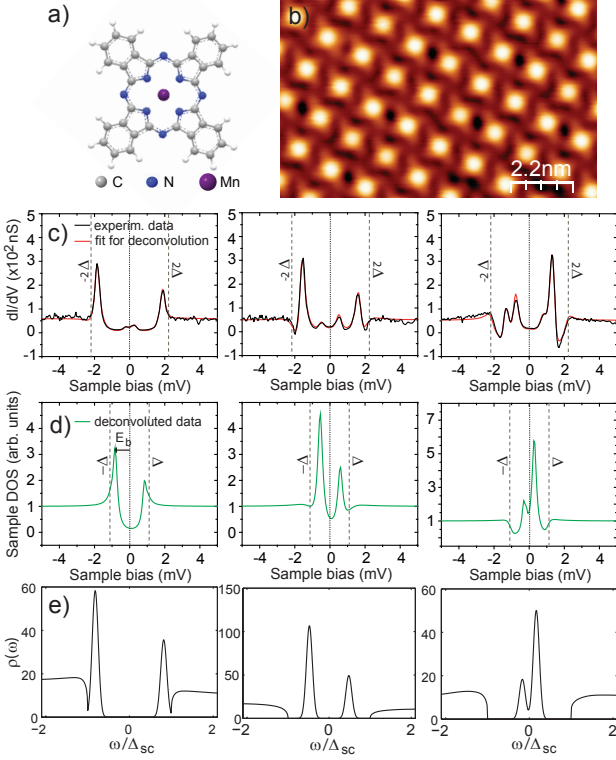


FIG. 1: (Color online) a) Molecular structure of Manganese-Phthalocyanine (MnPc), b) Constant-current STM image of highly ordered island of MnPc on Pb(111) ( $I = 23$  pA,  $U = 100$  mV), c) Tunneling spectra taken on different molecules on top of the Mn center (feedback opened at  $I = 450$  pA,  $U = 8.6$  mV). Also shown are the fits used to derive the deconvoluted spectra below in (d). e) Examples of NRG spectra with broadened peaks for similar  $E_b$ .

Fano lineshapes, representing two different Kondo screening processes with  $T_{K,2} \gg T_{K,1}$  [13]. For the isolated MnPc complex, density functional theory (DFT) calculations have found that the high spin configuration of Mn ( $S = 5/2$ ) is reduced to  $S = 3/2$  and the unpaired electrons occupy the  $b_{2g}(d_{xy})$ , the  $e_g(d_{\pi})$ , and the  $a_{1g}(d_{z^2})$  orbital ( $x$ -axis along an arm of MnPc) and are aligned due to Hund's rule coupling [22]. When adsorbed on the Pb surface (in  $z$  direction), the  $d_{z^2}$  orbital hybridizes strongly with the Pb states and is therefore quenched [23]. Hence, two screening channels and a spin  $S = 1$  is left. Since  $k_B T_{K,2} \gg \Delta_{sc}$ , Kondo screening dominates for this channel [7]. Therefore, we only correlate  $T_{K,1} = T_K \sim \Delta_{sc}$  with the appearance of the BS.

Three differential conductance spectra taken on different MnPc molecules are shown in Fig. 1(c). Two larger peaks as well as the two smaller peaks are located at symmetric bias voltages, while their intensity shows a strong asymmetry. Similar to the zero bias peak in the plain superconductor-superconductor junction, the small peaks are a result of thermal excitations across the gap. In order to remove the effect of the superconducting tip on the tunneling spectra, we developed a deconvolution method [13]. The result is representative for the quasi-

particle density of states (DOS) of the MnPc molecule on the superconducting Pb surface (Fig. 1(d)). These plots serve to deduce  $E_b$  and their intensity. We observe a gradual increase in the asymmetry of the weights when the states shift closer to the Fermi level  $\varepsilon_F$ . This is shown in Fig. 2 as ratio  $w_{b,g}/w_{b,s}$ , where  $w_{b,g}$  is the larger weight and  $w_{b,s}$  the smaller one weight.

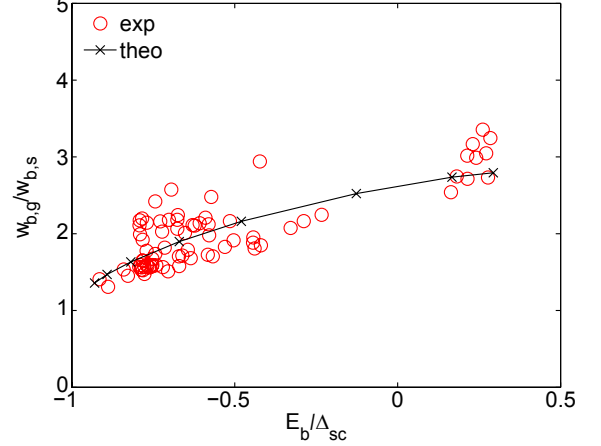


FIG. 2: (Color online) Ratio of bound state weights  $w_{b,g}/w_{b,s}$  vs bound state energy  $E_b/\Delta_{sc}$ . Comparison of experimental results with theory. In all the range of bound state energy we used the model parameters  $\varepsilon_d/\Delta_{sc} \approx -73$ , and  $U/\Delta_{sc} \approx 91$  and the overlap  $\Gamma$  was varied; we did not consider any further variation of  $\varepsilon_d, U$  which could lead to a better agreement in some cases.

Fig. 3 shows the dependence of  $E_b$  on  $R_{K,sc}$ . At large  $R_{K,sc}$ , the Kondo screening is efficient and the many-body ground state is a singlet. Here tunneling can occur via the doublet state which involves breaking of the Kondo singlet and rearrangement of Cooper pairs. With decreasing  $R_{K,sc}$  this requires less energy and we find  $E_b \rightarrow 0$ , and the BS and GS cross for  $R_{K,sc}^c \simeq 1.2$ . This point can be regarded as the critical point of the quantum phase transition and is a universal feature. Further decrease of  $R_{K,sc}$  leads to the unscreened doublet GS.

For the theoretical description we use an AIM Hamiltonian of the form

$$H = H_{sc} + H_d + H_{mix}. \quad (1)$$

The superconducting medium reads,

$$H_{sc} = \sum_{\mathbf{k}, m, \sigma} \varepsilon_{\mathbf{k}, m} c_{\mathbf{k}, m, \sigma}^\dagger c_{m, \mathbf{k}, \sigma} - \sum_{\mathbf{k}, m} (\Delta_{sc} c_{\mathbf{k}, m, \uparrow}^\dagger c_{-\mathbf{k}, m, \downarrow}^\dagger + \text{h.c.}) \quad (2)$$

where  $c_{\mathbf{k}, m, \sigma}^\dagger$  creates a band electron with momentum  $\mathbf{k}$ , spin  $\sigma$  and band index  $m$ , where  $m = 1, \dots, N$ , and there are  $N$  available channels.  $\varepsilon_{\mathbf{k}, m}$  is the corresponding electronic dispersion and  $\Delta_{sc}$  the gap parameter chosen real. The band electrons hybridize with the impurity states via

$$H_{mix} = \sum_{\mathbf{k}, m, \sigma} (V_m c_{\mathbf{k}, m, \sigma}^\dagger c_{d, m, \sigma} + \text{h.c.}), \quad (3)$$

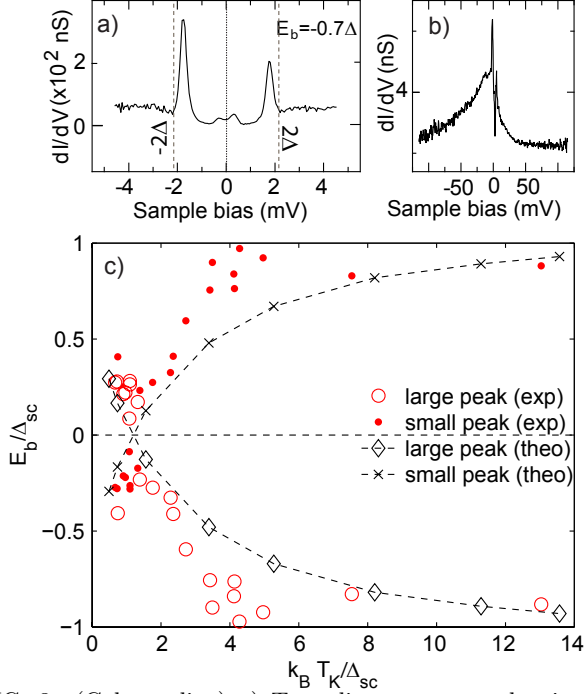


FIG. 3: (Color online) a) Tunneling spectrum showing the Shiba states (feedback opened at  $I = 450$  pA,  $U = 8.6$  mV). b) Tunneling spectrum on the same molecule as in (a) in a larger energy scale evidencing a Kondo resonance (feedback opened at  $I = 470$  pA,  $U = 130$  mV). c) Bound state energies  $E_b/\Delta_{sc}$  vs Kondo temperature  $T_K/\Delta_{sc}$ . Comparison of experimental results with theory for the same choice of model parameters as in Fig. 2.

where  $c_{d,m,\sigma}^\dagger$  creates a d-level impurity electron with spin  $\sigma$  and index  $m$ . We will assume different matrix elements  $V_m$  due to different overlapping integrals. We define the width  $\Gamma_m = \pi V_m^2 \rho_{m,c}$  as the energy scale for the hybridization,  $\rho_{m,c}$  is the DOS of the conduction band at  $\varepsilon_F$ . We will now show that the experimental results can be well described by a single channel model ( $N = 1$ ). In this case the “d-orbital” term  $H_d$  simply reads,

$$H_d = \sum_{\sigma} \varepsilon_d n_{\sigma} + U n_{\uparrow} n_{\downarrow}, \quad (4)$$

with the level position  $\varepsilon_d$  relative to  $\varepsilon_F$  and the on-site interaction with strength  $U$ , where  $n_{\sigma} = c_{d,\sigma}^\dagger c_{d,\sigma}$ . We set  $\varepsilon_F = 0$  in the following. The superconducting gap  $\Delta_{sc} = 1.1$  meV is fixed and sets the energy scale in all calculations. Even though the charge degrees of freedom of the impurity do not play a role at low energy, we stick to the description in terms of an AIM. The asymmetry of the weights  $w_b$  can then be captured by a deviation from particle-hole symmetry,  $\xi = \varepsilon_d/U + 1/2 \neq 0$ . Alternatively one could use a Kondo model with a potential scattering term.

The choice of model parameters is motivated by the expectation that the main difference for the MnPc molecules in the different positions is the magnitude of

the hybridization  $\Gamma$ , which in turn leads to different  $J$  and  $T_K$ . The energy  $\varepsilon_d$  and the asymmetry  $\xi$  are, on the contrary, expected to change little with the site [24]. Calculations for a set of parameters  $\varepsilon_d/\Delta_{sc} \approx -73$ , and  $U/\Delta_{sc} \approx 91$ , and varying  $\Gamma/\Delta_{sc}$  from 16 – 46 lead to an appropriate variation of  $E_b$  and  $w_b$  in Fig. 2 and give suitable Kondo scales in Fig. 3. Good agreement of theory and experiment is obtained both for universal features such as  $R_{K,sc}^c$  and non-universal ones like  $w_{b,g}/w_{b,s}$ . Notice that  $w_{b,g}/w_{b,s}$  increases whilst  $\xi$  is constant. The smallest value for  $\Gamma$  corresponds to the lowest value of  $T_K$ , at the  $S = 1/2$  doublet GS. The energy asymmetry of the levels is with  $\xi \approx 0.3$  quite large. Other methods [19–21] can give asymmetric weights even in more symmetric situations, however, they are based on classical spins, such that the Kondo effect is not captured.

Notice that the magnitudes of  $\varepsilon_d$ ,  $U$  and  $\Gamma$  do not correspond to usual atomic values  $\sim O(eV)$ , but rather to values of the order 100 meV. This is related to the fact that the AIM under consideration is an effective model valid for low energies (see discussion later). Calculations with  $\varepsilon_d$ ,  $U \sim O(eV)$  produce a less pronounced increase of  $w_{b,g}/w_{b,s}$  and can not explain the data very well.

Of particular interest is the occurrence of the quantum phase transition. At first sight the experimental result for this transition,  $R_{K,sc}^c \simeq 1.2$ , in Fig. 3 seems at odds with earlier theoretical predictions. For both the one channel non-degenerate AIM and the Kondo model, NRG studies [15–18] have estimated that it occurs when  $R_{K,sc}^c \simeq 0.3$ . We find that the origin of this discrepancy is the use of different definitions of  $T_K$ , which can vary by a prefactor. In the theoretical works [15–18] the definition [25]

$$T_K = 0.29[UT]^{1/2} e^{\frac{\pi \varepsilon_d(\varepsilon_d + U)}{2\Gamma U}}. \quad (5)$$

was used. In this work, we employ the definition of  $T_K$ , widely used in experiments [26, 27], based on the width of the Kondo resonance  $\Delta_K$  (half width at half maximum) in the limit  $T \rightarrow 0$ . We adopt the same definition in our NRG calculations ( $T_K = \Delta_K$ ) and find that  $\Delta_K$  and the definition in Eq. (5) can differ by a factor 4 (see also Ref. [28]). Taking this into account our result for the quantum phase transition in Fig. 3 is in excellent agreement with the theoretical prediction for a one channel model. If more channels contribute for a given value of  $T_K$ , the transition occurs at smaller values of  $R_{K,sc}^c$  [29] at variance with experiment.

We now discuss the emergence of the low energy effective one-channel model and the scaling of the model parameters. Using the DFT calculations for MnPc [22] as an input, we start with a model of the form of equation (1) with  $N=2$  and  $\Gamma_1 < \Gamma_2$ . Due to the spatial orientation the overlap is larger for the  $d_{\pi}$  orbital. The impurity term can be written in terms of the level positions  $\varepsilon_{d,m}$  relative to  $\varepsilon_F$ , intra orbital  $U_m$ , inter orbital Coulomb

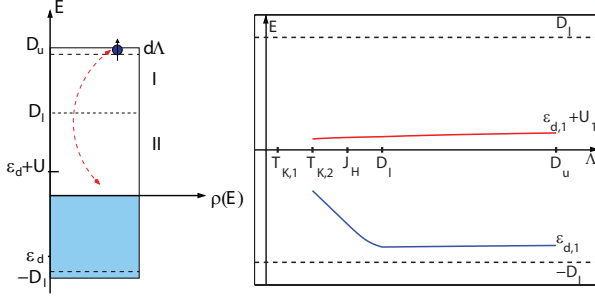


FIG. 4: (Color online) Left: Schematic plot of the bare band and impurity energy scales and depiction of two scaling regimes (I,II). Right: Schematic plot of the scaling of the effective level  $\varepsilon_{d,1}$  and  $\varepsilon_{d,1} + U_1$  in the two regimes  $\Lambda \in (D_l, D_u)$  and  $\Lambda \in (T_{K,2}, D_l)$ . Scaling stops at  $\Lambda \sim T_{K,2}$ , and the effective one band model is used to compute the low energy properties.

interaction  $U_{12}$  and a Hund's rule interaction  $J_H$ ,

$$H_d = \sum_{\sigma,m} \varepsilon_{d,m} c_{d,m,\sigma}^\dagger c_{d,m,\sigma} + \sum_m U_m n_{d,m,\uparrow} n_{d,m,\downarrow} \quad (6)$$

$$+ \sum_{\sigma,\sigma'} U_{12} n_{d,1,\sigma} n_{d,2,\sigma'} - J_H \mathbf{S}_{d,1} \cdot \mathbf{S}_{d,2},$$

where  $S_{d,m}^\alpha = \sum_{\sigma_1,\sigma_2} c_{d,m,\sigma_1}^\dagger \sigma_{\sigma_1,\sigma_2}^\alpha c_{d,m,\sigma_2}$  with the Pauli matrix  $\sigma^\alpha$ . The bare parameters of this model are not known, either from theoretical calculations or from experimental observations. However, generally we must have  $\varepsilon_{d,m} + U_{12} < 0$  and  $\varepsilon_{d,m} + U_{12} + U_m > 0$  such that single occupation is favored.

We now derive poor man's scaling equations [30] for the occupied level  $\varepsilon_{d,m}$  and the interaction  $U_m$  [25]. We focus on the quantities in channel 1. We only consider processes  $\sim V_1^2$  explicitly, where the level occupations of  $\varepsilon_{d,1}$  changes. There are also contributions  $\sim V_2^2$ , whose inclusion leads to quantitative changes in the equations but does not alter the conclusions. Band structure calculations [31] for Pb suggest a situation, where the band  $(-D_l, D_u)$  is asymmetric with respect to  $\varepsilon_F$ ,  $D_l < D_u$ . Then, we have two scaling regimes (I,II, see Fig. 4), and the scaling equations (I) for  $\Lambda \in (D_l, D_u)$  read [9, 25],

$$\frac{d\varepsilon_{d,1}}{d\Lambda} \simeq \frac{\Gamma_1}{\pi} \frac{1}{\Lambda - \varepsilon_{d,1}}, \quad (7)$$

$$\frac{dU_1}{d\Lambda} \simeq \frac{2\Gamma_1}{\pi} \frac{U_1}{(\Lambda - \varepsilon_{d,1})(\Lambda - \bar{\varepsilon}_{d,1})}, \quad (8)$$

where  $\bar{\varepsilon}_{d,1} = \varepsilon_{d,1} + U_1$ . Different from the usual approaches we also use a scaling equation for  $\Gamma_1$ , which is derived from  $dT_{K,1}/d\Lambda = 0$ , assuming  $T_{K,1}$  as a scaling invariant. Such a scaling procedure can be continued as long as the levels  $\varepsilon_{d,1}$ ,  $\varepsilon_{d,1} + U_1$  lie within  $(-\Lambda, \Lambda)$  and do not interfere with the Kondo scale. For  $|\varepsilon_{d,1}| < \Lambda$ ,  $|\varepsilon_{d,1} + U_1| < \Lambda$ , we find  $\frac{d\varepsilon_{d,1}}{d\Lambda} > 0$ . This implies that the level  $\varepsilon_{d,1}$  is decreasing when scaling to lower energy. We also have  $\frac{dU_1}{d\Lambda} > 0$  and  $\frac{d(\varepsilon_{d,1} + U_1)}{d\Lambda} > 0$ , such that  $(\varepsilon_{d,1} + U_1)$

decreases under the scaling. Hence, the model becomes more asymmetric in this regime.

Once  $\Lambda \sim D_l$  scaling changes to the equations (II),

$$\frac{d\varepsilon_{d,1}}{d\Lambda} \simeq \frac{\Gamma_1}{\pi} \frac{2\varepsilon_{d,1}(\varepsilon_{d,1} + \Lambda) + U_1(3\varepsilon_{d,1} - \Lambda)}{(\Lambda^2 - \varepsilon_{d,1}^2)(\Lambda + \bar{\varepsilon}_{d,1})}, \quad (9)$$

$$\frac{dU_1}{d\Lambda} \simeq \frac{4\Gamma_1}{\pi} \frac{\bar{\varepsilon}_{d,1}(\Lambda^2 - \varepsilon_{d,1}^2) - \varepsilon_{d,1}(\Lambda^2 - \bar{\varepsilon}_{d,1}^2)}{(\Lambda^2 - \varepsilon_{d,1}^2)(\Lambda^2 - \bar{\varepsilon}_{d,1}^2)}.$$

For starting values,  $\varepsilon_{d,1}(D_l) < 0$ ,  $\varepsilon_{d,1}(D_l) + U_1(D_l) > 0$ , and  $|\varepsilon_{d,1}| < D_l$ ,  $|\varepsilon_{d,1} + U_1| < D_l$ , one has  $\frac{d\varepsilon_{d,1}}{d\Lambda} < 0$ . In this case  $\varepsilon_{d,1}$  is increasing under the scaling. For the same effective starting values we have  $\frac{dU_1}{d\Lambda} > 0$ . Hence,  $U_1$  and  $(\varepsilon_{d,1} + U_1)$  decrease further under the scaling. This scaling can be continued until we reach  $\Lambda \sim J_H$ . We have  $T_{K,2} \sim 50 \text{ meV}$ ,  $D_l \sim 3 \text{ eV}$ , thus for usual estimates for  $J_H$  we expect  $T_{K,2} < J_H < D_l$ . At this scale the spins lock into the high spin  $S = 1$  configuration. As shown in Ref. [32], this leads to a reduction of the magnetic coupling  $J \rightarrow J/(2S)$  and the Kondo scale. In our approach it can be included in  $\Gamma_1$ , such that the scaling is slowed down [32]. Scaling can then be continued until  $\Lambda \sim T_{2,K}$ . Then one part of the impurity spin becomes Kondo screened and decouples. At this scale we have an effective single band model with  $S = 1/2$ . According to the described scaling procedure, the parameters are substantially reduced from the bare values and generically asymmetric. This justifies our choice of parameters in the NRG calculations.

In conclusion, we provide a unified experimental and theoretical perspective of the microscopic interplay of Kondo screening and superconducting pairing for MnPc on lead, as manifested in the subgap bound states. We show that in spite of the complexity of MnPc an effective description based on the one channel AIM captures both universal aspects like  $R_{K,sc}^c$  and non-universal ones like the asymmetry of the weights very well. In the future it would be interesting to envisage situations, where the impurity spins can interact, such that different kinds of quantum phase transitions can occur.

*Acknowledgments* - We wish to thank P. Coleman, M. Haverkort, A.C. Hewson, A. Subedi for helpful discussions and G. Schulze for the deconvolution program of tunneling spectra. We thank the Focus area Nanoscale of Freie Universität Berlin and the Deutsche Forschungsgemeinschaft through Sfb 658 for financial support.

- 
- [1] A. A. Abrikosov and L. P. Gorkov, Sov. Phys. JETP **12**, 1243 (1961).
  - [2] J. Zittartz and E. Müller-Hartmann, Z. Physik. **232**, 11 (1970).
  - [3] J. Zittartz, Z. Physik. **237**, 419 (1970).
  - [4] E. Müller-Hartmann and J. Zittartz, Phys. Rev. Lett. **26**, 428 (1971).

- [5] H. Shiba, Prog. Theor. Phys **50**, 50 (1973).
- [6] T. Matsuura, Prog. Theor. Phys. **57**, 1823 (1979).
- [7] A. V. Balatsky, I. Vekhter, and J.-X. Zhu, Rev. Mod. Phys. **78**, 373 (2006).
- [8] J. Kondo, Prog. Theor. Phys **32**, 37 (1964).
- [9] A. C. Hewson, *The Kondo Problem to Heavy Fermions* (Cambridge University Press, Cambridge, 1993).
- [10] A. Sakurai, Prog. Theor. Phys. **44**, 1472 (1970).
- [11] R. S. Deacon, Y. Tanaka, A. Oiwa, R. Sakano, K. Yoshida, K. Shibata, K. Hirakawa, and S. Tarucha, Phys. Rev. Lett. **104**, 076805 (2010).
- [12] A. Yazdani, B. A. Jones, C. P. Lutz, M. F. Crommie, and D. M. Eigler, Science **275**, 1767 (1997).
- [13] K. J. Franke, G. Schulze, and J. I. Pascual, Science **332**, 940 (2011).
- [14] R. Bulla, T. Costi, and T. Pruschke, Rev. Mod. Phys. **80**, 395 (2008).
- [15] K. Satori, H. Shiba, O. Sakai, and Y. Shimizu, J. Phys. Soc. Japan **61**, 3239 (1992).
- [16] O. Sakai, Y. Shimizu, H. Shiba, and K. Satori, J. Phys. Soc. Japan **62**, 3181 (1993).
- [17] T. Yoshioka and Y. Ohashi, J. Phys. Soc. Japan **69**, 1812 (2000).
- [18] J. Bauer, A. Oguri, and A. Hewson, J. Phys.: Cond. Mat. **19**, 486211 (2007).
- [19] M. E. Flatté and J. M. Byers, Phys. Rev. Lett. **78**, 3761 (1997).
- [20] M. E. Flatté and J. M. Byers, Phys. Rev. B **56**, 11213 (1997).
- [21] M. I. Salkola, A. V. Balatsky, and J. R. Schrieffer, Phys. Rev. B **55**, 12648 (1997).
- [22] M.-S. Liao, J. D. Watts, and M.-J. Huang, Inorganic Chemistry **44**, 1941 (2005).
- [23] Y.-S. Fu, S.-H. Ji, X. Chen, X.-C. Ma, R. Wu, C.-C. Wang, W.-H. Duan, X.-H. Qiu, B. Sun, P. Zhang, et al., Phys. Rev. Lett. **99**, 256601 (2007).
- [24] S.-H. Ji, et al., Chin. Phys. Lett. **27**, 087202 (2010).
- [25] F. D. M. Haldane, Phys. Rev. Lett. **40**, 416 (1978).
- [26] D. Goldhaber-Gordon, et al., Phys. Rev. Lett. **81**, 5225 (1998).
- [27] K. Nagaoka, et al., Phys. Rev. Lett. **88**, 077205 (2002).
- [28] T. A. Costi, Phys. Rev. Lett. **85**, 1504 (2000).
- [29] R. Žitko, O. Bodensiek, and T. Pruschke, Phys. Rev. B **83**, 054512 (2011).
- [30] P. W. Anderson, J. Phys. C **3**, 2435 (1970).
- [31] A. D. Zdetsis, E. N. Economou, and D. A. Papaconstantopoulos, Journal of Physics F: Metal Physics **10**, 1149 (1980).
- [32] A. H. Nevidomskyy and P. Coleman, Phys. Rev. Lett. **103**, 147205 (2009).